XENON: A 1 TONNE LIQUID XENON EXPERIMENT FOR A SENSITIVE DARK MATTER SEARCH

E. APRILE, T. BALTZ, A. CURIONI, K-L. GIBONI, C. HAILEY, L. HUI, M. KOBAYASHI, K. NI
Columbia University
E-mail: age@astro.columbia.edu

W. CRAIG
Lawrence Livermore National Laboratory

R. GAITSKELL
Brown University

U. OBERLACK
Rice University

T. SHUTT
Princeton University

Dark Matter

1 Introduction

Substantial astronomical evidence shows that at least 90% of the mass in the universe is dark, and that most of it is non-baryonic in nature (see e.g. reviews [1,2,3,4]). Dark matter plays a central role in current structure formation theories, and its microscopic properties have a significant impact on the spatial distribution of mass, galaxies and clusters. Unraveling the nature of dark matter is therefore of critical importance. Several lines of arguments indicate that the dark matter consists of Weakly Interacting Massive Particles (WIMPs), a well-motivated example of which is the neutralino, the lightest supersymmetric particle. Direct detection, via elastic scattering of a WIMP on a suitable target, offers the hope of studying the dark matter properties in detail, and shedding light on particle physics beyond the Standard Model.

In spite of the experimental challenges, a number of efforts worldwide are actively pursuing to directly detect WIMPs with a variety of targets and approaches. One approach is to decrease the radioactive background to extreme low levels, using a high purity Germanium target and detector, with careful selection of surrounding materials [5,6,7]. A second approach, followed by the

DAMA [8] and the UKDM NAIAD [9] groups, has been to use large NaI scintillators with pulse shape background discrimination. The third experimental approach relies on more powerful discrimination methods, using various schemes to extract as much information as possible from the target-detector. To this class belong the cryogenic detectors based on the simultaneous measurement of ionization and phonons in crystals of Ge or Si, as used by the CDMS experiment [10] and the EDELWEISS experiment [11], or phonons and scintillation light in $CaWO_4$ crystals as used by the CRESST experiment [12]. Experiments based on the simultaneous detection of ionization and scintillation light in liquid xenon (LXe) belong to the same class and offer an equally promising approach to direct detection of WIMPS in large scale targets. Two experiments, ZEPLIN II[13] and III[14], 30 kg and 6 kg of Xe mass, respectively, are currently being developed as part of the UKDM LXe program. Scale-up to the 1-tonne level is in the planning or proposal stage [14,15].

The XENON project, recently proposed to NSF for an initial development phase, is an alternative concept for a 1-tonne LXe experiment, to be located in the National Underground Science Laboratory (NUSL), under discussion in the US. The goal of the XENON experiment is to achieve a factor of 30 higher sensitivity than that projected for CDMS II [16] in the US and other experiment in Europe (e.g. EDELWEISS). This sensitivity increase is needed to probe the lowest SUSY predictions for the neutralino. With 1-tonne target mass, a visible energy threshold of 4 keV and a background discrimination factor much better than 99.5%, XENON projected sensitivity is 0.0001 events/kg/day after 3 yr operation.

2 Liquid Xenon for Dark Matter

Liquid xenon is an attractive target for a sensitive WIMP search. Its high density ($\sim$ 3 g/cm^3) and high atomic number (Z = 54, A = 131) allow for a compact detector geometry. The high mass of the Xe nucleus is favorable for WIMP scalar interactions, provided a low recoil energy threshold. Fig. 1 shows the expected event rate, integrated above the energy threshold, in Xe, Ge and S, for a 100 GeV WIMP with a cross-section $\sigma = 3.6\ 10^{-42}$ cm^2. For a threshold of $\sim$ 16 keV the expected rate is 1 event/kg/day.

As detector material LXe has excellent ionization and scintillation properties. With the simultaneous measurement of charge and light and 3D position resolution, event information can be maximized to achieve effective and redundant background identification and discrimination power, while maintaining most of the target active. Xenon, which contains both odd and even isotopes for coherent and purely spin-dependent WIMP interactions, is available in

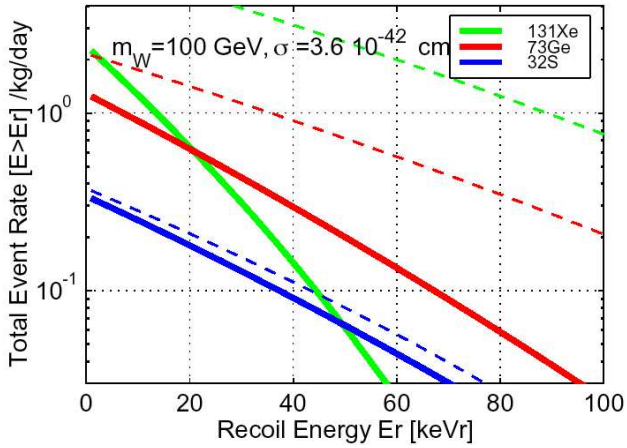

Figure 1. Expected event rate, integrated above energy threshold, for Xe, Ge and S, for a 100 GeV WIMP with cross section $\sigma = 3.6\ 10^{-42}$ cm^2.

large quantities at reasonable cost. Various techniques have demonstrated ultra pure LXe in which an electron lifetime in excess of 1 ms [17,18,19] allows the drift of free electrons over 30 cm and longer. The reduction of the krypton contamination in natural xenon to the required part per billion (ppb) level has also been verified with a distillation tower and cold traps.

3 The XENON Experiment: Design Overview

The XENON design is modular. An array of 10 independent 3D position sensitive liquid xenon time projection chambers (LXeTPC) makes the 1-tonne scale experiment. Each TPC contains 100 kg of active Xe mass and is self-shielded with additional LXe scintillator, as schematically shown in Fig. 2.

The modular approach is preferred over a single detector, for several reasons. The most important is a feasibility argument. We have already built a 30 kg LXeTPC and have used it for several balloon flights of the Liquid Xenon Gamma-Ray Imaging Telescope (LXeGRIT) [20,21,22,23,24,25,26]. In this TPC, with a maximum drift gap of 10 cm, both charge and light signals are detected for imaging gamma-rays. The excellent background discrimination which directly stems from the 3D event localization in the homogeneous volume has been demonstrated. The experience gained though this development effort, and the prior years of R&D on noble liquid detectors (e.g.[27,17,28,29,30]),

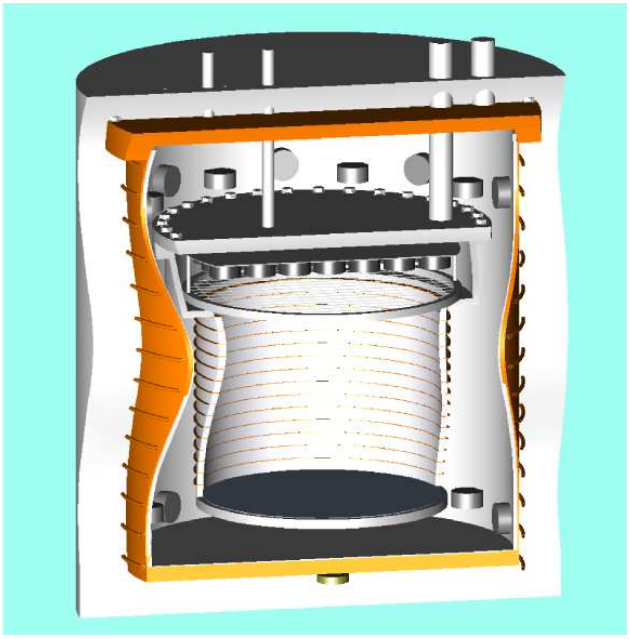

Figure 2. The LXeTPC module for XENON: the 100 kg fiducial target is surrounded by an active LXe shield enclosed in the Cu vessel.

give us the confidence that a 100 kg TPC optimized for dark matter can be built successfully. An array of independent detectors is also favored from a safety and risk factor point of view. Finally, with an array, a failure of one module would not halt the entire experiment. Operational efficiency is clearly higher than with a monolithic detector of 1-tonne.

As shown in details in Fig. 3, the LXeTPC structure containing the active Xe target is formed by a sandwich of Teflon spacers as UV diffuse reflector and thin copper rings for electric field shaping. The structure is closed at the bottom by a thin copper plate. The inside of this plate is coated with CsI as photocathode to convert Xe scintillation photons into free electric charges. The structure forms a 30 cm high cylinder with 38 cm inner diameter, holding about 100 kg of ultra pure liquid xenon.

On the top, the structure is hermetically sealed to a cylindrical copper vessel of larger diameter, housing the PMTs and the wire structure for the proportional scintillation process in the gas phase.

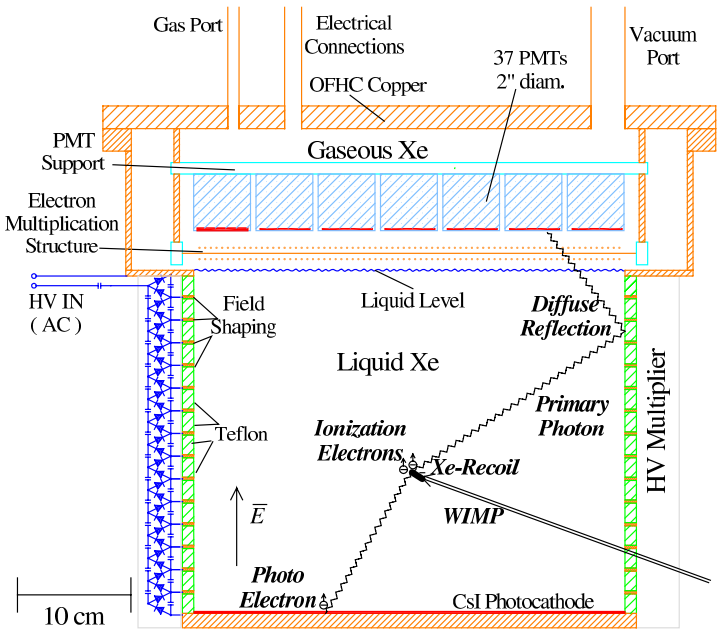

Figure 3. The LXeTPC module for XENON: Schematic Design of the 100 Kg detector and its components.

The LXeTPC structure is enclosed in a copper vessel containing the liquid xenon for active shielding. With both detectors at the same temperature and similar pressure, the amount of material for the inner detector walls is minimized. The scintillation light from the shield section is viewed by two rings of PMTs.

3.1 The XENON LXeTPC: Principle of Operation

Referring to Fig. 3, which shows in more details the TPC design, we limit the discussion to the relevant processes in LXe which are used to detect and discriminate a WIMP from background.

The elastic scattering of a WIMP within the active target results in a low energy Xe recoil. The moving recoil produces both ionization electrons and fast UV scintillation photons at 178 nm, from the de-excitation to the ground state of excited diatomic Xe molecules (Xe_2^*).

The number of UV photons associated with direct Xe excitation by a

nuclear recoil is only a fraction of that emitted by an electron or gamma-ray with the same kinetic energy. Recent measurements of this 'quenching factor' for Xe scintillation range from about 22% [31] to 45% [32]. The number of free electrons liberated by a nuclear recoil is also very small, even if a strong electric field is applied across the liquid [27,33], because the bulk of the ionization electrons recombine within picoseconds. The strong recombination, characteristic of heavily ionizing particles in LXe, leads to the emission of more UV photons.

Thus, under a high electric field, a nuclear recoil will yield a very small charge signal and a much larger light signal. On the other hand, an electron recoil of the same energy, will yield the opposite. The distinct charge/light ratio is the basis for nuclear recoil discrimination in a LXe detector. To detect the small charge signals involved, the process of electroluminescence [34] is typically used. The free ionization electrons are extracted from the liquid to the gas phase where in the strong field around thin wires they induce proportional scintillation light. The number of photons generated by one drifting electron results in a large amplification factor, allowing a simple PMT to detect the small number of free electrons extracted from the liquid. Results obtained with small size dual phase LXe prototypes have demonstrated the power of the method [35] and motivate the ongoing efforts to use LXe for a direct WIMP search with high sensitivity. The challenge ahead lies in detecting both charge and light signals with high efficiency down to the lowest energy threshold. Furthermore, this has to be realized in a detector of sizeable scale and with the highest ratio of active/passive LXe.

These considerations have guided our design of the XENON TPC. In the baseline concept the primary UV photons are detected by an array of PMTs placed above the liquid-gas interface. To increase the solid angle and thus detection efficiency, a CsI photocathode immersed in the liquid is used to convert downwards heading photons into photoelectrons. The efficient extraction of photoelectrons from CsI in liquid rare gases was originally demonstrated by the Columbia group [36].

To further increase the primary light collection efficiency, which ultimately determines the detector energy threshold, the TPC walls are made of Teflon which has about 90% diffuse reflectivity at 178 nm [37]. At the liquid-gas interface, the charges are extracted into the gas phase and are detected via the proportional scintillation signal induced around thin wires (Fig. 5 shows the expected number of photoelectrons for a 16 keV "true" nuclear recoil. The CsI readout contributes the largest fraction).

Most events will provide three signals, shown schematically in Fig. 3.1. The first is the prompt scintillation signal detected directly by the PMTs and

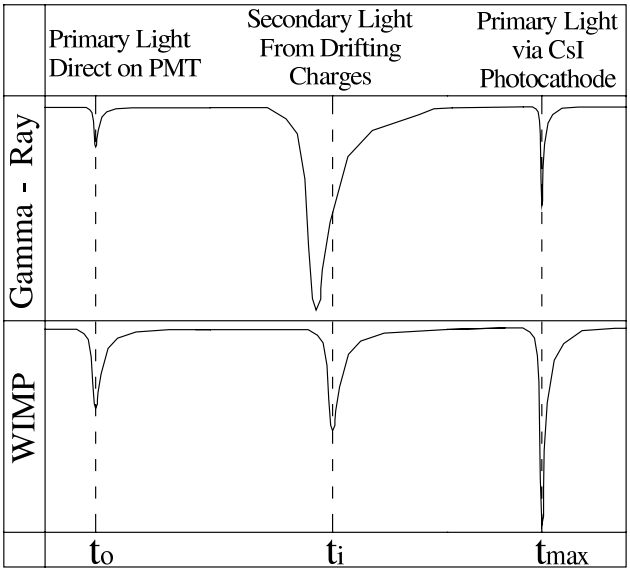

Figure 4. Shaped light profiles from an electron recoil (top) and nuclear recoil (bottom) in the XENON LXeTPC.

the last is the proportional scintillation signal from the CsI photoelectrons drifting the entire 30 cm liquid gap. The two signals are separated by exactly 150 μs. The proportional scintillation signal from the drift of ionization electrons can occur anywhere in between the other two. The difference in arrival time between the primary scintillation pulse and the proportional pulse from the electron drift measures the interaction depth (Z-coordinate) of the event. Since electron diffusion in LXe is small, the proportional scintillation pulse is produced in a small spot with the same X-Y coordinates as the interaction site. The photons in the proportional scintillation will spread over several PMTs in the vicinity of this spot. By a center of gravity method, the X-Y position can be reconstructed to about 1 cm precision. The X-Y information, along with the absolute Z, gives a 3D localization which will permit further background discrimination via fiducial volume cuts. For the rare events of low energy, it is possible that the first pulse is below detection threshold. The third pulse, however, will be seen since the CsI has high quantum efficiency and the signal is amplified by proportional scintillation. The Z-coordinate can still be inferred from the relative drift time difference, since the third pulse

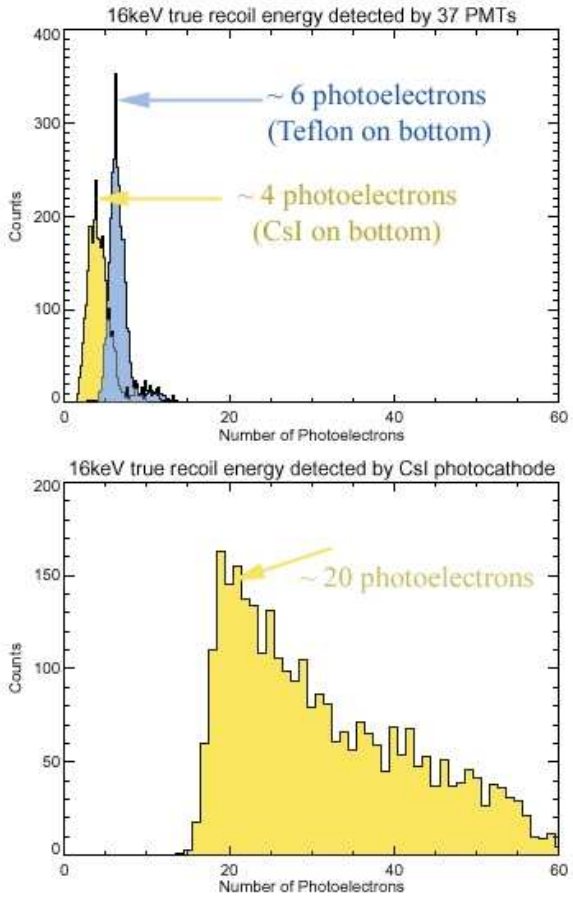

Figure 5. Number of photoelectrons for a 16 keV nuclear recoil. *Top:* as seen by the PMTs, *bottom:* extracted from the CsI photocathode.

contains the same information as the first. In addition, one can characterize events with incomplete signatures, by looking also at the sum signal from the wire structure, which will be present only if a proportional scintillation pulse is detected. Based on the redundant signal information allowed by our design and the 3D position sensitivity, we expect to achieve a background rejection efficiency better than 99.5% and energy threshold as low as few keV.

4 Background Considerations

To maximize the benefit of the various background rejection factors available for the XENON experiment, the absolute count rate itself must be minimized. This is a challenge for any WIMP experiment, as the possible sources of background are numerous and of different origin. Here, we limit the discussion to the dominant sources specific to a LXe experiment. Natural Xe has no long-lived isotopes. However, radioactive impurities in the gas, most notably ^{85}Kr, must be reduced by a large amount.

4.1 Gamma and Beta Induced Background

^{85}Kr and Radon – Commercially available, research grade xenon gas, typically has a Krypton fraction of 5-10 ppm. Kr has two long-lived radioisotopes, ^{81}Kr and ^{85}Kr. Due to its longer lifetime and smaller abundance, the background from ^{81}Kr is weaker than that from ^{85}Kr by a factor of several 10^5. Most of the ^{85}Kr found in the environment today was released by nuclear-fuel reprocessing plants, as a fission product of ^{235}U and ^{239}Pu. Its abundance is $\sim 2\times10^{-11}$ [38]. The ^{85}Kr β-decays with an endpoint energy of 678 keV. With a half-life of 10.8 yr, the residual signal in the XENON detector energy band is $\sim$ 20 cts/kg/d/keV. Reducing this to $\sim 1 \times 10^{-5}$ cts/kg/d/keV, with the assumed rejection power of the detector, requires a purity of Kr in Xe of 1 ppb. This can be achieved by distillation and cold traps. The ^{85}Kr level will be monitored in a similar way as in the BOREXINO experiment [39], namely through the delayed gamma-rays of a rare decay [40]. Radon, continuously produced by the decay chain of uranium contained in detector materials, will also be effectively removed with gas re-circulation and cold traps.
^{136}Xe double beta decay – Assuming a lifetime of 8×10^{21} years and Q=2.48 MeV we can use the double beta spectrum and directly calculate the fraction of events in our energy band of interest. The resulting count rate is 1×10^{-6} cts/kg/d/keV, which is small compared to other sources of background. And this is the count rate before any rejection cuts are applied.

4.2 Neutron Induced Background

Neutrons are a major source of background because their nuclear recoils render them indistinguishable from WIMP events. Nuclear recoils in the 10 keV range arise from the elastic scattering of 0.1- 10 MeV neutrons on Xe. With an active anti-coincidence, neutrons recoiling both in the LXe shield and the TPC LXe target are effectively identified and rejected. Nevertheless, underground operation and a sufficient neutron shield to absorb or at least thermalize the

environment neutrons are essential for a WIMP experiment. The main sources of neutrons are:
Muon Induced Neutrons – Cosmic ray muons produce neutrons in the Xe target and other materials by spallation. The primary concern is muon induced spallation of ^{136}Xe and ^{134}Xe, leading to ^{135}Xe and ^{133}Xe respectively. These spallations dominate because their abundances are about 10 times larger than for other Xe isotopes. Both γ-rays and β particles are produced in these spallations. We assume that the spallation cross-section is $\sim$ 10 mb. With the neutron production rate for Homestake's depth (4.4 kmwe), and accounting for the geometry of the detector, we calculate a total neutron production rate of 0.01 cts/kg/d and a differential count rate of 6×10^{-5} cts/kg/d, before background rejection. This source of background is therefore not a problem, and can be further reduced by a muon veto. With a modest 99% veto efficiency for muons, we expect to reduce the rate to $< 5 \times 10^{-6}$ cts/kg/d/keV. One is left then with neutrons from very high energy muons, penetrating through the experiment.
(α, n) *neutrons from surrounding rock* – The incoming neutron flux, due to (α, n) reactions from U and Th decay in the surrounding rock, will be $\sim$ 1000 n/m^2/d. To suppress this source of background, a liquid scintillator shield is required. Typically, a 20 cm shield can suppress the background to a level of 1×10^{-5}. The overall background from this source is estimated at $\sim 1 \times 10^{-6}$ cts/kg/d/keV.
Neutrons from U/Th contamination in the detector and surrounding materials – Within the shielding, further neutrons arise from the U/Th in the materials of the active TPC and of the active shield and its vessel. A reasonable estimate based on current understanding of relevant materials is $\sim 5 \times 10^{-5}$ cts/kg/d/keV and an aggressive goal, with higher purity materials, would be 5×10^{-6} cts/kg/d/keV.

4.3 Gamma–Rays from PMTs

Gamma-ray background from the same U/Th and K in most detector materials will dominate the overall count rate. PMTs, in particular, are typically a copious source of gamma-rays. The K/U/Th content is highest in the HV divider chain. The baseline XENON LXeTPC uses special PMTs, stripped of the standard divider chain and with selected compact metal envelopes and quartz windows. The radioactivity is estimated at $\sim$ 100 cts/d.

Table 1 summarizes the count rates from the main background listed above. These numbers reflect the 99.5% background factor based on nuclear recoil discrimination, but not the additional suppression which comes from

Background Source	Count Rate (kg^{-1} d^{-1} keV^{-1})
^{85}Kr	1×10^{-5}
^{136}Xe $\beta\beta$ Decay	$< 1 \times 10^{-6}$
Muon Spallation of Xe	$< 5 \times 10^{-6}$
Neutrons from Rock	1×10^{-6}
U / Th Neutrons	$0.5 - 5 \times 10^{-5}$
γ - Rays from PMTs	1.5×10^{-4}

Table 1. Expected count rates for the most important background sources in the XENON detector.

an active LXe shield, and fiducial volume cuts. Our sensitivity calculation (Sec. 5) has assumed a modest reduction factor of 10 in the PMTs gamma-rays rate, beyond that indicated in Table 1 due to the active LXe shield. While the neutron background will also be reduced to some degree by the shield, we have not taken this into account. The Table 1 numbers were specifically calculated for the Homestake site.

5 Experimental Sensitivity

The predicted sensitivity of the XENON experiment is shown in Fig. 6 along with that of other experiments: DAMA [8], NAIAD [9], HDMS[6], CDMS I [10], EDELWEISS [11], CRESST II [12], CDMS II [16], GENIUS [7]. The prediction of minimal SUSY is also plotted [41]. The calculation has been done for a 1000 kg fiducial target and for 3 years of operation. We have assumed that the acceptance of the detector for real WIMPS is ~ 1. The assumed overall background rate, as discussed in Sec. 4 is 3.9×10^{-5} cts/kg/d/keV. The fraction of misidentified candidate events was taken as $\varepsilon_g = 0.5\%$, based on 99.5% nuclear recoil discrimination based on light and charge in LXe. We have also assumed that the systematic uncertainty on ε_g is controlled at the 10% level, and the statistical limit therefore applies. The energy band was taken as 10 keV with a visible energy threshold of 4 keV. We converted the visible energy to recoil energy assuming that the quenching factor for Xenon is 0.25. The optimal energy bandwidth is a tradeoff between the background level, the form factor and the energy-dependent background misidentification.

Our sensitivity estimate does not yet take into account the additional

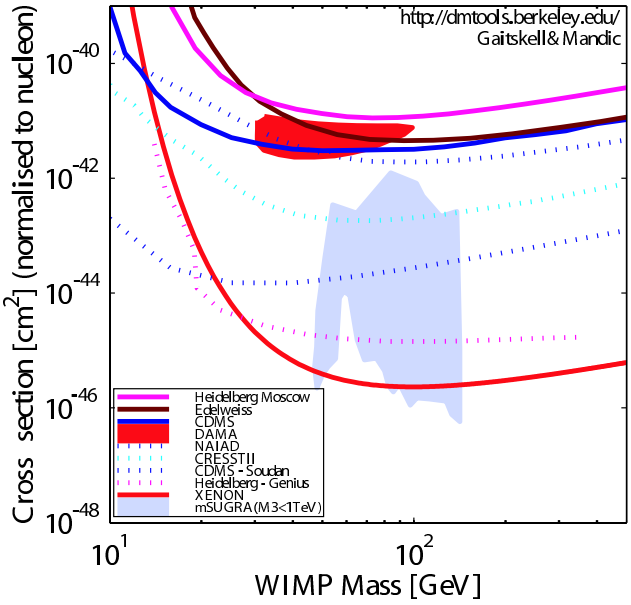

Figure 6. Achieved and projected limits for spin independent couplings as a function of WIMP mass

background suppression expected from 3D event localization. Finally, alternative photodetectors (LAAPD) or a charge redout based on GEMs, also part of our studies, would have the advantage of substantially lower the internal background. An improvement of about a factor of 4 or more depending on readout scheme and the efficiency of the self-shield of the XENON detectors is expected.

Conclusions

Acknowledgments

References

1. V. Trimble, ARA&A 25 (1987) 425–472.
2. J. R. Primack, D. Seckel, B. Sadoulet, Ann.Rev. Nucl. Part. Sci. 38 (1988) 751.
3. S. Tremaine, Physics Today 45 (1992) 28–36.

4. G. Jungman, M. Kamionkowski, K. Griest, Phys. Rept. 267 (1996) 195–373.
5. H. V. Klapdor-Kleingrothaus, et al. in: Proceedings of the Third International Workshop on the Identification of Dark Matter, World Scientific, 2000, pp. 415–420.
6. L. Baudis, et al., Physical Review D 59 (1999) 022001/1.
7. L. Baudis, et al., Physics Reports 307 (1998) 301–308.
8. R. Bernabei, et al., Phys. Lett. B480 (2000) 23–31.
9. N. J. C. Spooner, et al., Phys. Lett. B473 (2000) 330–336.
10. R. Abusaidi, et al., Phys. Rev. Lett. 84 (2000) 5699.
11. A. Benoit, et al., Phys. Lett. B513 (2001) 15–22.
12. M. Bravin, et al., Astropart. Phys. 12 (1999) 107–114.
13. H. Wang, in: D. Cline (Ed.), Sources and Detection of Dark Matter and Dark Energy in the Universe: 4th International Symposium, Feb. 23-25, 2000, Physics and Astronomy, 2000, p. 453.
14. T. Sumner, in: Proceedings of the third International Workshop on the Identification of Dark Matter, World Scientific, 2000, pp. 603–605.
15. D. Cline, H. Wang, et al., A White Paper for Snowmass 2001 .
16. R. Schnee, 6th International Workshop on Topics in Astroparticle and Underground Physics .
17. E. Aprile, R. Mukherjee, M. Suzuki, NIM A 300 (1991) 343.
18. E. Aprile, A. Bolotnikov, D. Chen, R. Mukherjee, F. Xu, NIM A Accepted.
19. P. Benetti, et al., NIM A 329 (1993) 361.
20. E. Aprile, et al., Proc. of SPIE 2806 (1996) 337–348.
21. E. Aprile, et al., NIM A 412 (1998) 425–436.
22. E. Aprile, et al., in: M. L. McConnell, J. M. Ryan (Eds.), The Fifth Compton Symposium, Vol. 510 of AIP Conf. Proc., AIP, New York, 2000, pp. 799–803.
23. E. Aprile, et al., in: K. A. Flanagan, O. H. W. Siegmund (Eds.), X-Ray and Gamma-Ray Instrumentation for Astronomy XI, Vol. 4140 of Proc. of SPIE, 2000, pp. 344–359, astro-ph/0012398.
24. E. Aprile, A. Curioni, K.-L. Giboni, U. Oberlack, S. Ventura, IEEE Trans. Nucl. Sci. Accepted (astro-ph/0012276).
25. U. G. Oberlack, E. Aprile, A. Curioni, V. Egorov, K.-L. Giboni, in: R. B. James, R. C. Schirato (Eds.), Hard X-Ray, Gamma-Ray, and Neutron Detector Physics II, Vol. 4141 of Proc. of SPIE, 2000, pp. 168–177, astro-ph/0012296.
26. U. Oberlack, E. Aprile, A. Curioni, K. L. Giboni, IEEE Trans. Nucl. Sci. Accepted (astro-ph/0012395).

27. E. Aprile, R. Mukherjee, M. Suzuki, IEEE Trans. Nucl. Sci. 37 (1990) 553–558.
28. E. Aprile, R. Mukherjee, M. Suzuki, NIM A 302 (1991) 177.
29. E. Aprile, D. Chen, M. Moulson, R. Mukherjee, M. Suzuki, NIM A 316 (1992) 29.
30. E. Aprile, A. Bolotnikov, D. Chen, R. Mukherjee, NIM A 327 (1993) 216.
31. F. Arneodo, et al., NIM A 449 (2000) 147.
32. R. Bernabei, et al., EPJC, to be published .
33. E. Aprile, R. Mukherjee, M. Suzuki, NIM A 307 (1991) 119.
34. A. Bolozdynya, NIM A 422 (1999) 314–320.
35. H. Wang, Phys. Rep. 307 (1998) 263.
36. E. Aprile, et al., NIM A 338 (1994) 328–335.
37. M. Yamashita, T. Doke, K. Kawasaki, J. Kikuchi, S. Suzuki, 2000 IEEE Nuclear Science Symposium. Conference Record (2000) 6/155.
38. P. Collon, et al., NIM B 123 (1997) 122.
39. Borexino Collaboration, to be published in Astroparticle Physics. Preprint hep-ex/0012030 .
40. G. Alimonti, et al., NIM A 406 (1998) 411.
41. V. Mandic, A. Pierce, P. Gondolo, H. Murayama, hep-ph/0008022